PHYSICAL REVIEW B **78**, 024106 (2008)

Identification of microscopic spin-polarization coupling in the ferroelectric phase of magnetoelectric multiferroic $CuFe_{1-x}Al_xO_2$

Taro Nakajima* and Setsuo Mitsuda
Department of Physics, Faculty of Science, Tokyo University of Science, Tokyo 162-8601, Japan

Toshiya Inami
Japan Atomic Energy Agency, Koto, Sayo-cho, Sayo-gun, Hyogo, 679-5148, Japan

Noriki Terada
ICYS, National Institute for Materials Science, Tsukuba, Ibaraki 305-0044, Japan

Hiroyuki Ohsumi
RIKEN SPring-8 Center, 1-1-1 Kouto, Sayo-cho, Sayo-gun, Hyogo 679-5148, Japan

Karel Prokes and Andrei Podlesnyak
Helmholtz-Centre Berlin for Materials and Energie, SF-2, Glienicker Strasse 100, Berlin 14109, Germany
(Received 24 April 2008; published 10 July 2008)

We have performed synchrotron radiation x-ray and neutron diffraction measurements on magnetoelectric multiferroic $CuFe_{1-x}Al_xO_2$ (x=0.0155), which has a proper helical magnetic structure with incommensurate propagation wave vector in the ferroelectric phase. The present measurements revealed that the ferroelectric phase is accompanied by lattice modulation with a wave number $2q$, where q is the magnetic modulation wave number. We have calculated the Fourier spectrum of the spatial modulations in the local electric polarization using a microscopic model proposed by T. Arima [J. Phys. Soc. Jpn. **76**, 073702 (2007)]. Comparing the experimental results with the calculation results, we found that the origin of the $2q$-lattice modulation is not the conventional magnetostriction but the variation in the metal-ligand hybridization between the magnetic Fe^{3+} ions and ligand O^{2-} ions. Combining the present results with the results of a previous polarized neutron diffraction study [Nakajima *et al.*, Phys. Rev. B **77**, 052401 (2008)], we conclude that the microscopic origin of the ferroelectricity in $CuFe_{1-x}Al_xO_2$ is the variation in the metal-ligand hybridization with spin-orbit coupling.

DOI: 10.1103/PhysRevB.78.024106 PACS number(s): 75.80.+q, 75.25.+z, 77.80.−e

I. INTRODUCTION

Magnetically induced ferroelectricity or electric control of magnetic ordering has been intensively investigated since a colossal magnetoelectric (ME) effect was found in $TbMnO_3$.[1] Recent experimental studies have discovered a variety of ferroelectric magnetic compounds, which might be suitable for use in advanced ME devices. These materials are often termed ME multiferroics. In order to develop practical device applications, it is essential to determine the microscopic mechanism of spin-polarization coupling in these systems. So far, there have been two different microscopic models for magnetically induced ferroelectricity. One is the spin-current model,[2] which predicts that two noncollinearly aligned neighboring spins $\boldsymbol{S}_i$ and $\boldsymbol{S}_{i+1}$ generate a local electric dipole moment $\boldsymbol{p}$ given by $\boldsymbol{p} \propto \boldsymbol{e}_{i,i+1} \times (\boldsymbol{S}_i \times \boldsymbol{S}_{i+1})$, where $\boldsymbol{e}_{i,i+1}$ is the unit vector connecting the two spins. This formula predicts macroscopic uniform electric polarization in a magnetic structure with cycloidal-spin components, and shows excellent agreement with the experimentally determined relationships between magnetic structures and electric polarization in various transition metal oxides, such as $TbMnO_3$,[3] $Tb_{1-x}Dy_xMnO_3$,[4] $Ni_3V_2O_8$,[5] $MnWO_4$,[6] and $CoCr_2O_4$.[7] The other microscopic model is the magnetostriction model, which predicts ferroelectricity in collinear commensurate magnetic structures. In this case, the local electric dipole moment is given by $C(\boldsymbol{r})(\boldsymbol{S}_i \cdot \boldsymbol{S}_{i+1})$, where $C(\boldsymbol{r})$ is a constant dependent on the local crystal structure and the exchange interactions. The spontaneous electric polarization observed in the collinear commensurate magnetic orderings in orthorhombic $HoMnO_3$ (Ref. 8) may be attributed to this model. However, there are several ME multiferroic materials whose ferroelectricity cannot be explained by either of these models,[9] for example, delafossite multiferroic $CuFeO_2$.[10–12] Hence, identification of microscopic spin-polarization coupling in these systems paves the way for a new design of multiferroic materials.

The crystal structure of $CuFeO_2$ is shown in Figs. 1(a)–1(c). Owing to the geometrical frustration in the triangular lattice planes of the magnetic Fe^{3+} ions, $CuFeO_2$ exhibits various magnetically ordered phases.[13–15] The ground state of $CuFeO_2$ is a collinear commensurate four-sublattice (4SL) antiferromagnetic state. A spontaneous electric polarization emerging in the direction perpendicular to the hexagonal c axis was discovered in the first field-induced phase.[10] Subsequent studies[16,17] revealed that the ferroelectric phase is stabilized even under zero field by substituting a small amount of nonmagnetic Al^{3+} ions for magnetic Fe^{3+} ions, as seen in Fig. 2. Recent neutron diffraction measurements in applied field revealed that the ferroelectric phase

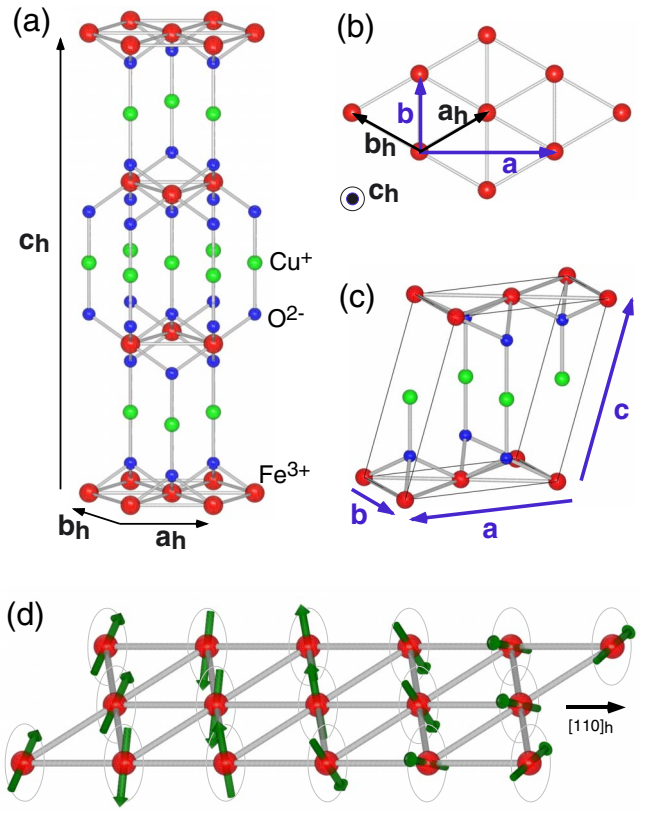

FIG. 1. (Color online) (a) Crystal structure of $CuFeO_2$ with the hexagonal basis $(\boldsymbol{a}_h,\boldsymbol{b}_h,\boldsymbol{c}_h)$. (b)-(c) Relationship between the hexagonal basis and the monoclinic basis $(\boldsymbol{a},\boldsymbol{b},\boldsymbol{c})$. (d) Schematic drawing of the proper helical magnetic structure in $CuFe_{1-x}Al_xO_2$.

magnetic structure is an antiferromagnetically stacked proper helical magnetic structure.[11] The wave vector is incommensurate. The helical axis is parallel to the hexagonal [110] direction, as shown in Fig. 1(d). Hereafter, we refer to the ferroelectric phase as the ferroelectric incommensurate (FEIC) phase. Since neither the spin-current model nor the magnetostriction model is able to explain the ferroelectricity in proper helical magnetic ordering, we anticipate that another type of spin-polarization coupling is realized in $CuFe_{1-x}Al_xO_2$.

Recently, Arima[18] presented a theoretical consideration on the ferroelectricity in $CuFe_{1-x}Al_xO_2$, suggesting that the variation in the metal-ligand hybridization with spin-orbit coupling is relevant to the ferroelectricity in this system. Applying a microscopic theory derived by Jia *et al.*[19,20] to a cluster model with a proper helical spin arrangement, Arima[18] has predicted the following intrinsic features of the ferroelectricity in this system: (i) the direction of the uniform polarization should be parallel to the helical axis of the proper helical magnetic ordering. (ii) the spin helicity (i.e., right- or left-handed helical arrangement of spins) should correspond to the polarity of the uniform polarization. (iii) There must be spatial modulations with wave numbers of $2q$ and $4q$ (where q is the magnetic modulation wave number) in the helical-axis components of the local electric polarization vectors.

The results of recent polarized neutron diffraction measurements on $CuFe_{1-x}Al_xO_2$ (x=0.02) under an applied electric field show excellent agreement with features (i) and (ii).[12] However, the existence of spatial modulations of the local polarization [feature (iii)] has not yet been confirmed. Spatial modulations of the local polarization must result in lattice modulations, which can be observed by x-ray diffraction measurements. The existence of incommensurate lattice modulations has been reported in the field-induced FEIC phase of undiluted $CuFeO_2$ by Terada *et al.*[21] and Ye *et al.*[22] However, application of a magnetic field readily induces slight distortion of the magnetic structure, as well as the uniform magnetization components. Actually, higher harmonic magnetic reflections have been detected in the field-induced FEIC phase of $CuFeO_2$.[14] As discussed by Terada *et al.* in Ref. 21, this situation can easily cause additional lattice modulations through magnetostriction. In order to elucidate the existence of the lattice modulations predicted by the metal-ligand hybridization model [feature (iii)], it is essential to remove the contribution of these field-induced lattice modulations.

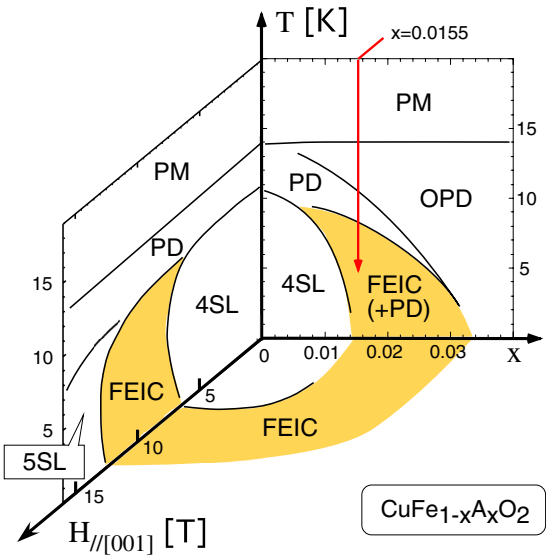

FIG. 2. (Color online) Schematic drawing of x-H-T phase diagram of $CuFe_{1-x}Al_xO_2$.

In the present study, we have performed synchrotron radiation x-ray measurements using a $CuFe_{1-x}Al_xO_2$ (x =0.0155) sample, which exhibits a FEIC phase under zero field. The present measurements reveal the existence of $2q$-lattice modulations in the zero-field FEIC phase. We have also investigated the magnetic-field dependence of the $2q$-lattice modulations by x-ray and neutron diffraction measurements under a field applied along the helical axis. In order to identify the origin of the observed $2q$-lattice modulation, we calculate the Fourier spectrum of the spatial modulations in the helical-axis component of the local electric polarization using the microscopic model presented by Arima.[18] This calculation reveals that the lattice modulation does not originate from a conventional magnetostriction but rather from the variation in the metal-ligand hybridization between the magnetic Fe^{3+} ions and the ligand O^{2-} ions. As a result, we conclude that the microscopic mechanism of the ferroelectricity in $CuFe_{1-x}Al_xO_2$ is the variation in the metal-ligand hybridization with spin-orbit coupling.

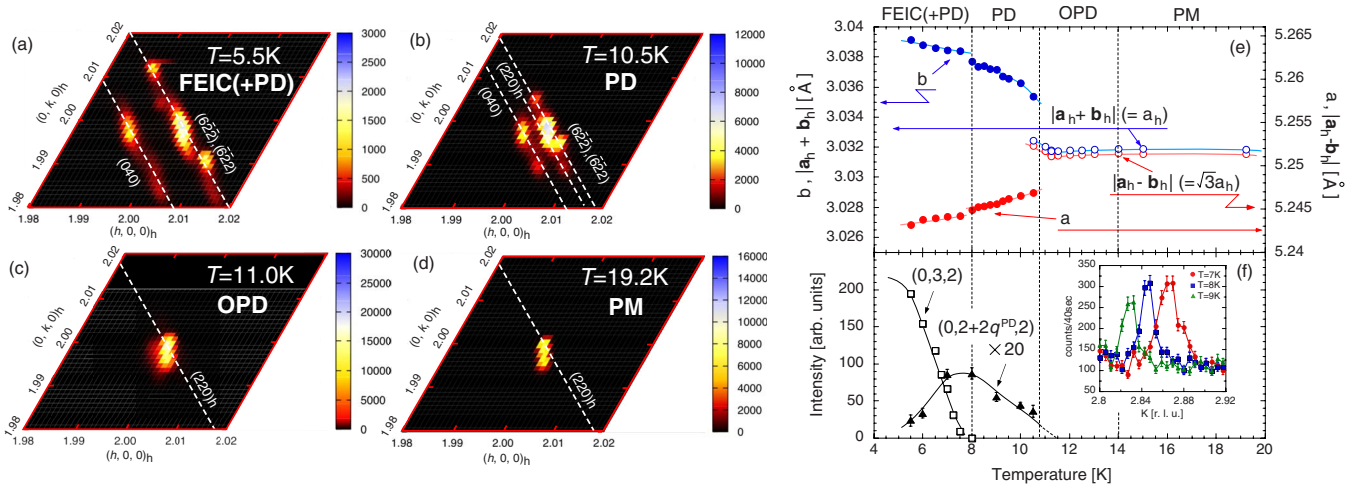

FIG. 3. (Color online) The x-ray diffraction intensity maps obtained by the $(H,K,0)_h$ reciprocal lattice scans around the reciprocal lattice position of $(2,2,0)_h$ at (a) $T=5.5$ K, (b) $T=10.5$ K, (c) $T=11.0$ K, and (d) $T=19.2$ K. These intensity maps were measured in a warming process. (e) Temperature variations of the lattice constants a and b in the monoclinic notation, which were measured on heating. (f) Temperature variations of the intensities of (0, 3, 2) and $(0,2+2q^{\mathrm{PD}},2)$ reflections. The inset shows the diffraction profiles of the $(0,2+2q^{\mathrm{PD}},2)$ reflections at typical temperatures. The data of $(0,2+2q^{\mathrm{PD}},2)$ are magnified by a factor of 20.

II. EXPERIMENTAL DETAILS

A single crystal of $CuFe_{1-x}Al_xO_2$ with $x=0.0155$ was prepared by the floating zone technique,[23] and was cut into a disk shape. The Al concentration was determined by chemical analysis. We performed x-ray diffraction measurements in zero field at the beamline BL46XU in SPring-8. The energies of the incident x-ray beams were tuned to 12 keV. The sample was mounted in a closed-cycle ^{4}He refrigerator. The data obtained in this measurement are presented in Sec. III A.

We have also performed x-ray diffraction measurements in zero field and in fields applied along the hexagonal [110] (monoclinic b axis) at the beamline BL22XU in SPring-8. The sample was mounted in a horizontal-field cryomagnet whose maximum field is 6 T; the hexagonal (hhl) plane was used as the scattering plane. The data obtained in these measurements are presented in Secs. III B and III C.

Neutron diffraction measurements in a field applied along the hexagonal [110] axis were performed at the two-axis neutron diffractometer E4 installed at the Berlin Neutron Scattering Center in Hahn-Meitner Institute. The hexagonal (hhl) plane was selected as the scattering plane. Incident neutrons with wave numbers of 2.44 Å were obtained by a pyrolytic graphite (002) monochromator. An external magnetic field directed along the hexagonal [110] direction was provided by the horizontal-field cryomagnet, HM-2, whose maximum field is 4 T.

As described later, $CuFe_{1-x}Al_xO_2$ with $x=0.0155$ exhibits a symmetry-lowering structural transition from a rhombohedral structure to a structure with lower symmetry (probably monoclinic symmetry, but possibly even lower symmetry). Taking into account the monoclinic lattice distortions found in the magnetically ordered phases of undiluted $CuFeO_2$,[22,24,25] it is reasonable to employ a monoclinic basis in addition to the conventional hexagonal basis. The definitions of these bases are shown in Figs. 1(a)–1(c). We mainly employed the monoclinic notation. To distinguish between the two bases, the subscript "h" has been added to the hexagonal notation when referring to modulation wave numbers and reciprocal lattice indices.

III. EXPERIMENTAL RESULTS

A. Characterization of the crystal structures in the magnetically ordered phases

Before discussing the lattice modulations in the ferroelectric phase, we present the symmetry-lowering structural transition corresponding to the magnetic phase transitions in $CuFe_{1-x}Al_xO_2$ with $x=0.0155$. At first, we should review the magnetic phase transitions in the $x=0.0155$ sample.[26] As shown in Fig. 2, this system exhibits three magnetically ordered phases in zero field. For all the phases, the magnetic modulation wave vectors are described by $(0,q,\frac{1}{2})[=(q_h,q_h,\frac{3}{2})_h]$. The highest temperature phase and the intermediate phase are the oblique partially disordered (OPD) phase and the partially disordered (PD) phase, respectively. Both of them have collinear sinusoidal magnetic structures with incommensurate wave numbers. The wave number of the OPD phase, $q^{\mathrm{OPD}}\sim 0.390$, is independent of temperature, while that of the PD phase, q^{PD}, varies with temperature $(0.404<q^{\mathrm{PD}}<0.430)$. The lowest temperature phase is the FEIC phase, whose modulation wave number is $q^{\mathrm{FEIC}}=0.414$.

Figures 3(a)–3(d) show the x-ray diffraction intensity maps around the reciprocal lattice position of $(2,2,0)_h$ in the paramagnetic (PM) phase and the magnetically ordered phases. As seen in Fig. 3(d), a single peak assigned as $(2,2,0)_h$ is observed at $T=19.2$ K in the PM phase. In the PD and FEIC phases, this fundamental peak splits into several peaks, as shown in Figs. 3(a) and 3(b). This suggests that the threefold rotational symmetry along the c_h axis vanishes, resulting in a monoclinic (or even lower symmetry) lattice

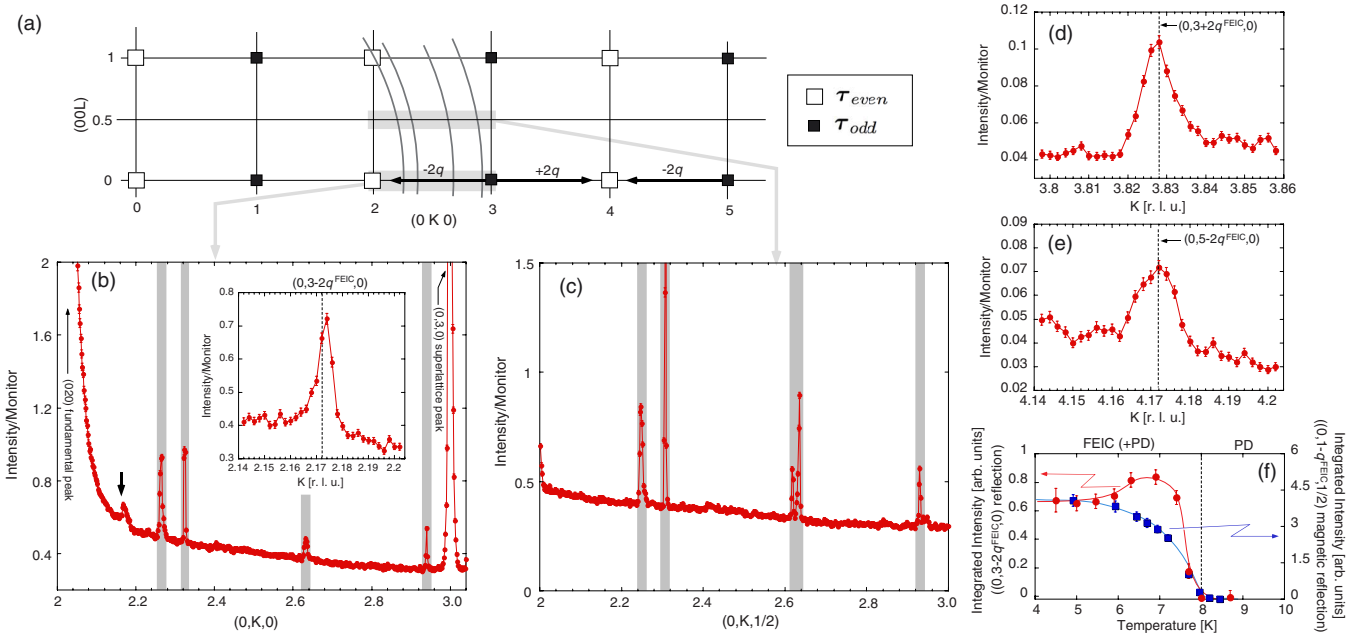

FIG. 4. (Color online) (a) Illustration of the reciprocal lattice $(0KL)$ zone. [(b)-(c)] Diffraction profiles of the (b) $(0K0)$ and (c) $(0K\frac{1}{2})$ reciprocal lattice scans in the FEIC phase. Contamination peaks from the Cu sample holder are masked by the shaded areas. The inset of (b) shows the magnification around the reciprocal lattice position of $(0,3-2q^{\mathrm{FEIC}},0)$. [(d)–(e)] The diffraction profiles of (d) $(0,3+2q^{\mathrm{FEIC}},0)$ and (e) $(0,5-2q^{\mathrm{FEIC}},0)$ reflections. (f) Temperature dependences of the integrated intensity of the $(0,3-2q^{\mathrm{FEIC}},0)$ reflection and the neutron diffraction intensity of the magnetic Bragg reflection corresponding to the FEIC magnetic ordering (taken from Ref. 26), under zero field.

distortion in the PD phase and the FEIC phase.

The monoclinic lattice distortions are also observed in the undiluted $(x=0.00)$ system,[24,25] in which the PD and FEIC phases show up as the thermally induced phase and the first field-induced phase, respectively. As discussed in the previous studies,[22,24,25] these structural transitions are due to the bond order induced by the magnetostriction, which leads to magnetic ordering with lower symmetry and lifts the macroscopic degeneracy of the magnetic states.

On the other hand, splitting of the $(2,2,0)_h$ peak was not observed in the OPD phase, as shown in Fig. 3(c), even though the magnetic structure of the OPD phase does not have threefold rotational symmetry along the c_h axis.[27] This suggests that the coherent bond order is not essential to the OPD magnetic ordering. Based on the fact that the OPD phase is never observed without nonmagnetic substitution, it is reasonable to propose that the OPD magnetic ordering is stabilized by local symmetry breaking due to the site-random magnetic vacancies.

Using the monoclinic basis, we can identify the splitting peaks in the FEIC and PD phases, as shown in Figs. 3(a) and 3(b), and we can also estimate the temperature variation of the lattice constants a and b in the $x=0.0155$ sample, as shown in Fig. 3(e). The differences between the lattice constants in the FEIC (or PD) phase and those in the PM phase in this system are comparable to those in the undiluted system.[22,24,25] These results suggest that the crystal structures of the FEIC and PD phases in the $x=0.0155$ sample are almost the same as those in the undiluted system.

In the present measurements, we observed incommensurate superlattice reflection at the reciprocal lattice point of (0, 2.86, 2) in the PD phase. This reflection can be assigned as $\boldsymbol{\tau}_{\mathrm{even}}+(0,2q^{\mathrm{PD}},0)$, where $\boldsymbol{\tau}_{\mathrm{even}}$ is the reciprocal lattice point of (H,K,L) with the condition "$H+K=2n$" (n is an integer). We also observed commensurate superlattice reflection at the reciprocal lattice points of (0, 3, 2) in the FEIC phase. The temperature variations of the intensities of these reflections are shown in Fig. 3(f). The incommensurate superlattice reflection in the PD phase and the commensurate superlattice reflection in the FEIC phase are also observed in the undiluted system,[21,22,25] and are consistently explained by the magnetostriction model proposed by Terada *et al.*[21]

B. Lattice modulations in the FEIC phase

We now focus on the incommensurate lattice modulations in the FEIC phase. Figures 4(b) and 4(c) show the x-ray diffraction profiles of the $(0,K,0)$ and $(0,K,\frac{1}{2})$ reciprocal lattice scans at $T=4.5$ K in the FEIC phase under zero field. As shown in Fig. 4(b) and its inset, a satellite reflection is found at the reciprocal lattice position of (0, 2.172, 0). The intensity of this reflection is smaller than that of the (0, 4, 0) fundamental reflection by a factor $10^{-7}\sim10^{-8}$. This reflection is successfully identified as being $(0,3-2q^{\mathrm{FEIC}},0)$. It should be noted that the experimental resolution in the present measurement can clearly distinguish the difference between the q^{FEIC} and q^{PD} phases at $T=4.5$ K (~0.43), although the high-temperature PD phase coexists with the FEIC phase under zero-field cooling in the $x=0.0155$ sample.[26,28] We confirmed the repetition of this reflection in reciprocal lattice space, as shown in the Figs. 4(d) and 4(e). Hereafter, we refer to these reflections as $\boldsymbol{\tau}_{\mathrm{odd}}\pm(0,2q^{\mathrm{FEIC}},0)$ reflections, where $\boldsymbol{\tau}_{\mathrm{odd}}$ is the reciprocal lattice point of (H,K,L) with the condition "$H+K=2n+1$."

The $\boldsymbol{\tau}_{\rm odd} \pm (0, 2q^{\rm FEIC}, 0)$ reflections are observed only in the FEIC phase. However, as shown in Fig. 4(f), the temperature variation of the integrated intensity of the $\boldsymbol{\tau}_{\rm odd} \pm (0, 2q^{\rm FEIC}, 0)$ reflection is not proportional to that of the magnetic order parameter; specifically, the intensity of the $(0, 3-2q^{\rm FEIC}, 0)$ reflection obviously increases around $T=6.5$ K with increasing temperature, and rapidly decreases at the transition temperature from the FEIC phase to the PD phase, $T=8$ K, while the FEIC magnetic order parameter (neutron diffraction intensity) monotonically decreases with increasing temperature, as seen in Fig. 4(f).

No significant reflections were detected in the $(0, K, \frac{1}{2})$ reciprocal lattice scan, as shown in Fig. 4(c). The satellite reflections assigned as $(0, 2n \pm q^{\rm FEIC}, \frac{1}{2})$ and $(0, (2n+1) \pm q^{\rm FEIC}, \frac{1}{2})$ were observed in the field-induced FEIC phase of undiluted $CuFeO_2$.[21] These satellite reflections indicate the existence of a lattice modulation with a wave number $1q^{\rm FEIC}$ in the field-induced FEIC phase. However, these reflections were not observed in the zero-field FEIC phase of $CuFe_{1-x}Al_xO_2$ with $x=0.0155$. This is consistent with the calculation of Terada *et al.*,[21] which shows that the combination of the proper helical-spin components and uniform magnetization components along the c_h axis induces $1q$-lattice modulation through magnetostriction, and suggests that the $1q$-lattice modulation is not essential to the ferroelectricity in this system.

The present results reveal that the $2q$-lattice modulation corresponding to the satellite reflections at $\boldsymbol{\tau}_{\rm odd} \pm (0, 2q^{\rm FEIC}, 0)$ exists in the zero-field FEIC phase. The microscopic origin of the $2q$-lattice modulation is discussed in Sec. IV.

C. $H_{\parallel b}$ dependence of the $2q$-lattice modulation

We also surveyed the magnetic field dependence of the $\boldsymbol{\tau}_{\rm odd} \pm (0, 2q^{\rm FEIC}, 0)$ reflections by the x-ray diffraction measurements under an applied field. As mentioned above, application of a magnetic field along the c_h axis readily leads to additional lattice modulations through magnetostriction. We thus applied a magnetic field along the helical axis of the proper helical magnetic structure, i.e., along the b axis. When a magnetic field is applied along this direction, the proper helical magnetic structure deforms into a conical magnetic structure, as shown in Fig. 5(d). In this configuration, the magnetic field ($H_{\parallel b}$) does not modify the amplitude of the magnetic moment at each Fe^{3+} site. Hence, the magnetostriction cannot induce additional lattice modulations.

Figure 5(a) shows the integrated intensity of the $(0, 3-2q^{\rm FEIC}, 0)$ reflection at $T=4.5$ K as a function of the magnetic field along the b axis ($H_{\parallel b}$). The intensity of the reflection increases with increasing magnetic field. This result leads to the following two possibilities: that the amplitude of the $2q$-lattice modulation itself increases with increasing magnetic field, or the fractions of the three magnetic domains, which reflect the threefold rotational symmetry of the original trigonal crystal structure, change with magnetic field intensity.

We have also performed $(0, K, 0)$ and $(0, K, \frac{1}{2})$ reciprocal lattice scans at $T=4.5$ K under $H_{\parallel b}=6$ T. In both these scans, no additional (field-induced) reflections are detected.

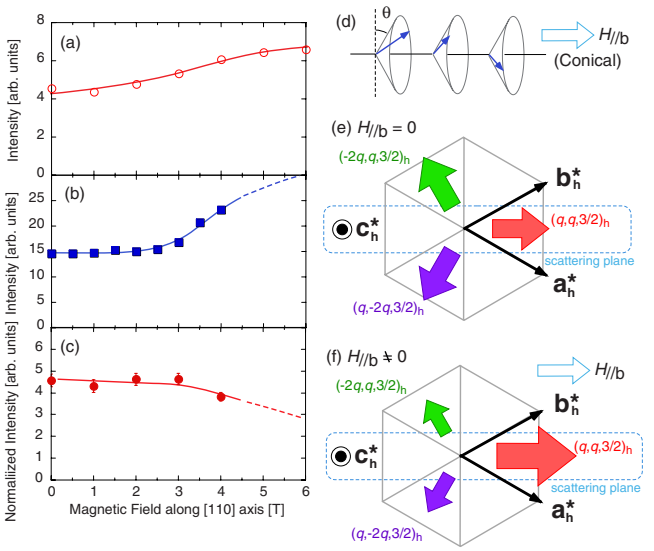

FIG. 5. (Color online) (a)The $H_{\parallel b}$ dependence of the integrated intensity of $(0, 3-2q^{\rm FEIC}, 0)$ reflection observed in the x-ray diffraction measurements. (b) The $H_{\parallel b}$-dependence of $(\frac{1}{2}-q_h^{\rm FEIC}, \frac{1}{2}-q_h^{\rm FEIC}, \frac{3}{2})_h$ magnetic Bragg reflection observed in the neutron diffraction measurements at $T=4.5$ K. (d) The field dependence of the integrated intensity of $(0, 3-2q^{\rm FEIC}, 0)$ reflection normalized by the data of the neutron diffraction measurements. (d) Schematic drawings of a conical structure with uniform magnetization component along the helical axis. [(e)–(f)] Schematic drawings of the fractions of three magnetic domains (e) under zero field, and (f) under applied field along the b axis ($[110]_h$ axis). The directions of the filled arrows denote the $[001]_h$ projections of the propagation wave vectors. The sizes of arrows qualitatively show the fractions of each domain.

D. Neutron diffraction measurements under applied field along the b axis

In order to elucidate the origin of the $H_{\parallel b}$ variation of the intensity of the $(0, 3-2q^{\rm FEIC}, 0)$ reflection, we performed neutron diffraction measurements under an applied field along the b axis. We found that the magnetic Bragg reflections corresponding to the FEIC magnetic ordering increase with increasing magnetic field.[29] Figure 5(b) shows the field dependence of the intensity of the $(\frac{1}{2}-q_h^{\rm FEIC}, \frac{1}{2}-q_h^{\rm FEIC}, \frac{3}{2})_h$ magnetic Bragg reflection, where $q_h^{\rm FEIC}[=\frac{1}{2}q^{\rm FEIC}]=0.207$. Since the change in the magnetic structure factor is considered to be negligible for magnetic fields of $0<H_{\parallel b}<4$ T,[28] this enhancement of the magnetic Bragg intensity indicates that the fraction of the FEIC magnetic domain increases with the propagation wave vector $(q_h^{\rm FEIC}, q_h^{\rm FEIC}, \frac{3}{2})_h$. This result supports the latter scenario for the enhancement of the intensity of the $(0, 3-2q^{\rm FEIC}, 0)$ reflection. A magnetic field along the b axis ($[110]_h$ axis) should favor the magnetic domain, in which a more uniform magnetization component is induced along the direction of the magnetic field. As a result, the fraction of the magnetic domains with a wave vector $(q_h, q_h, \frac{3}{2})_h$ is enhanced by the magnetic field along the $[110]_h$ axis, and the fractions of the other magnetic domains

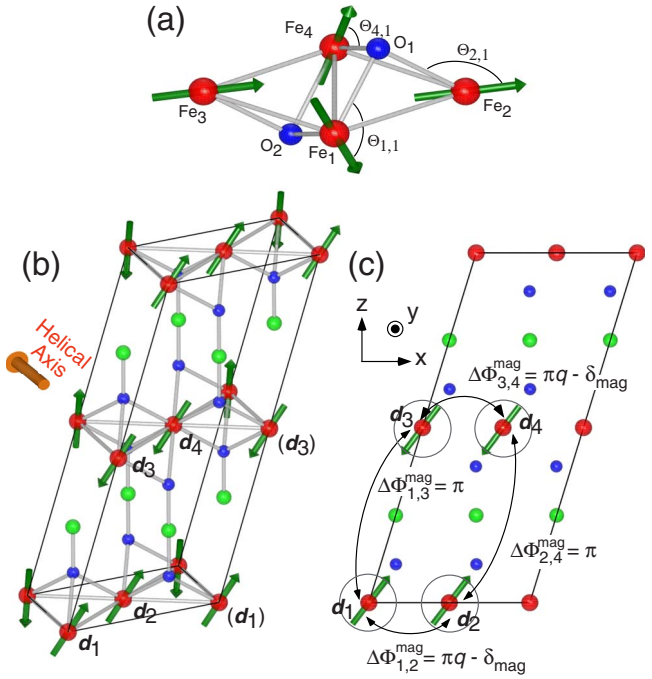

FIG. 6. (Color online) (a) A Fe_4O_2 cluster used for the calculation of the local electric dipole moment in Ref. 18. (b) The magnetic structure in the FEIC phase with the $a\times b\times 2c$ cell. (c) The phase differences in the magnetic modulations ($\Delta\Phi_{i,j}^{\mathrm{mag}}$) between the Fe^{3+} sites.

with the wave vectors $(-2q_h, q_h, \frac{3}{2})_h$ and $(q_h, -2q_h, \frac{3}{2})_h$ should be reduced, as shown in Figs. 5(e) and 5(f). The details of the magnetic domain distributions and the magnetic phase transitions in $CuFe_{1-x}Al_xO_2$ (x=0.0155) under applied field along the $[110]_h$, $[1\bar{1}0]_h$, and $[001]_h$ directions will be presented in another paper.[28]

Figure 5(c) shows the intensity of the $(0,3-2q^{\mathrm{FEIC}},0)$ reflection normalized to the intensity of the magnetic Bragg reflection. In the magnetic field region of $H_{\|b}\leq 4$ T, the amplitude of the $2q$-lattice modulation does not exhibit remarkable change, and it decreases slightly above $H_{\|b}=3$ T.

IV. DISCUSSIONS

A. Review of Arima's cluster model

In this section, we discuss whether the microscopic origin of the $2q$-lattice modulation observed in the FEIC phase is the variation in the d-p hybridization or not. At first, we start from the Fe_4O_2 cluster model used in Ref. 18 [see Fig. 6(a)]. Applying the microscopic theory by Jia *et al.*[19,20] to the Fe-O covalent bonding, Arima[18] pointed out that the d-p hybridization between a magnetic Fe^{3+} ion and a ligand O^{2-} ion is slightly modified depending on the direction of the magnetic moment at the Fe^{3+} site. As a result, the charge transfer from the magnetic Fe_i (i=1,2,3,4) site to the neighboring O_j (j=1,2) site can be described by

$$C_0 + \Delta C \cos 2\Theta_{i,j}, \tag{1}$$

where C_0 is the charge transfer in the PM phase, and ΔC is the constant dependant on the difference in the spin-orbit interaction between Fe_i and O_j, and the magnitude of the ordered magnetic moment at the Fe site, and so on. $\Theta_{i,j}$ is the angle between the direction of the Fe_i-O_j bond and the direction of the magnetic moment at the Fe_i site. The macroscopic uniform electric polarization is not induced by this term only. Arima[18] argued that the many-body effect among the three covalent Fe-O bonds, which are concerned with an O^{2-} ion, should be taken into account in Eq. (1). As shown in Fig. 6(a), an O^{2-} ion in this cluster (or $CuFeO_2$) is surrounded by three neighboring Fe^{3+} ions. Hence, the charge transfer between Fe_i and O_j should be slightly affected by the amount of charge transfer in the other two Fe-O bonds, which are concerned with the O_j site. For example, the covalency between O_1 and Fe_1 should be reduced when Fe_2-O_1 and Fe_4-O_1 bonds are more covalent. Taking account of this many-body effect, the charge transfer from Fe_1 to O_1 can be described as follows:[30]

$$C_0[1 + C'\cos 2\Theta_{1,1}][1 - \alpha C'(\cos 2\Theta_{2,1} + \cos 2\Theta_{4,1})], \tag{2}$$

where $C'=\Delta C/C_0(\ll 1)$. α is the parameter representing the efficiency of the many-body effect, and is assumed to be small $\alpha\ll 1$. Here, we apply to the cluster a proper helical magnetic structure with a modulation wave number q, whose helical axis is parallel to the Fe_1-Fe_4 bond direction. The helical-axis component of the induced electric dipole moment at the O_1 site, p_b, should be proportional to the imbalance between the charge transfer from Fe_1 to O_1 and that from Fe_4 to O_1,

$$p_b \propto (1+\alpha)(\cos 2\Theta_{1,1} - \cos 2\Theta_{4,1}) - \alpha C' \cos 2\Theta_{2,1}(\cos 2\Theta_{1,1} - \cos 2\Theta_{4,1}). \tag{3}$$

In the case of the proper helical magnetic structure, the value of $\cos 2\Theta_{i,j}$ oscillates with a period of half the magnetic modulation. As a result, the first term of Eq. (3) gives the nonuniform polarization oscillating with a wave number of $2q$ ($2q$ modulation), and the second term of Eq. (3) gives the uniform polarization and the nonuniform polarization oscillating with a wave number of $4q$ ($4q$ modulation). It should be noted that one can derive Eq. (6) in Ref. 18 from Eq. (3) in this paper. The above formula of the local electric polarization suggests that the amplitude of the $4q$ modulation is much smaller than that of the $2q$ modulation. In the limit of α=0, the uniform polarization and $4q$ modulation vanish. It is worth mentioning here that the same amount of electric dipole moment is induced at the O_2 site because of the symmetry of the proper helical magnetic structure.

B. Calculation results in zero field

We apply Eq. (3) to the magnetic structure in the FEIC phase, which has been determined by a previous magnetic structure analysis.[11] For simplicity, hereafter, we refer to the wave number and the wave vector in the FEIC phase as q and $\boldsymbol{q}[=(0,q,\frac{1}{2})]$, respectively. In order to define the spin arrangement in the FEIC phase, we employ $a\times b\times 2c$ cell, as shown in Fig. 6(b). This cell contains four Fe^{3+} sites, and the fractional coordinates of these sites are

$$\boldsymbol{d}_1 = (0,0,0),$$

$$\boldsymbol{d}_2 = (0,1/2,0),$$

$$\boldsymbol{d}_3 = (0,0,1),$$

$$\boldsymbol{d}_4 = (0,1/2,1). \tag{4}$$

From the results of a previous magnetic structure analysis, the spin components at $\boldsymbol{d}_i$ site are described, using the Cartesian coordinates shown in Fig. 6(c), as follows:

$$S_i^x = \mu_x \cos(2\pi \boldsymbol{q} \cdot (\boldsymbol{l} + \boldsymbol{d}_i) - \phi_i),$$

$$S_i^y = 0,$$

$$S_i^z = \mu_z \sin(2\pi \boldsymbol{q} \cdot (\boldsymbol{l} + \boldsymbol{d}_i) - \phi_i), \tag{5}$$

μ_x and μ_z are the magnetic moments along the x and z axes, respectively. Since no significant ellipticity has been detected in the magnetic structure analysis for zero field (and for relatively low fields, $H_{\parallel[001]_h} < 4$ T) on the $x=0.0155$ sample,[11] we assume at this stage that the magnetic structure has no ellipticity, i.e., $\mu_x = \mu_z = \mu$. ϕ_i is the relative phase shift at the $\boldsymbol{d}_i$ site; specifically,

$$|\phi_1 - \phi_2| = |\phi_3 - \phi_4| = \delta_{\mathrm{mag}},$$

$$|\phi_1 - \phi_3| = |\phi_2 - \phi_4| = 0. \tag{6}$$

Although δ_{mag} was determined to be $\sim 76°\,(\sim \pi q)$ by magnetic structure analysis,[11] we treat δ_{mag} as a parameter in the following calculation. Here, we define the phase difference of the magnetic modulations between the $\boldsymbol{d}_i$ site and the $\boldsymbol{d}_j$ site as $\Delta\Phi_{i,j}^{\mathrm{mag}}$. Using this notation, the relationship among the phases of the magnetic modulations on the four Fe^{3+} sites is summarized in Fig. 6(c).

We numerically calculated the spatial modulations of p_b at each oxygen site using Eq. (3). The system size is set to be $a \times Nb \times 2c$. Since the magnetic propagation wave number along the b axis is incommensurate, N is set to be a large number (typically, $N \sim 100$). We also calculated Fourier spectra for their nonuniform components. Here, we define the phase difference in the nq modulation ($n=2,4$) between the oxygen site neighboring $\boldsymbol{d}_i$ site and that neighboring $\boldsymbol{d}_j$ site, as $\Delta\Phi_{i,j}^{nq}$, in the same manner as that of the magnetic modulations. The results of the calculations for $\Delta\Phi_{i,j}^{2q}$ and $\Delta\Phi_{i,j}^{4q}$ are shown in Figs. 7(a) and 7(d). For the $2q$ modulations, there is a finite phase shift, $2\delta_{\mathrm{mag}}$, between the oxygen site neighboring the $\boldsymbol{d}_1$ ($\boldsymbol{d}_3$) site and that neighboring the $\boldsymbol{d}_2$ ($\boldsymbol{d}_4$) site. For the $4q$ modulation, there are no phase shifts along the a axis. For both of the $2q$ and $4q$ modulations, there are also no phase shifts along the c axis. These results are summarized in Figs. 7(c) and 7(d).

The intensities of the calculated Fourier spectra for the spatial modulations of p_b, $|P(\boldsymbol{Q})|^2$, where $\boldsymbol{Q}$ is a vector in the reciprocal lattice space, are mapped onto the reciprocal lattice space, as shown in Figs. 8(a) and 8(b). Since the d-p hybridization model predicts that the local electric polarization arises from the local imbalance of the Fe-O bond covalency, it is reasonable to consider that the spatial modulations of the local electric polarization result in spatial modulations of the local atomic displacements of the oxygen ions. We thus assume that the local displacement of the oxygen ion is proportional to the magnitude of the local polarization vector. In this case, $|P(\boldsymbol{Q})|$ is proportional to the structure factor in the x-ray diffraction measurements. In the case of $\delta_{\mathrm{mag}} = 0, \pi$, satellite peaks corresponding to the $2q$ and $4q$ modulations appear at $\boldsymbol{\tau}_{\mathrm{even}} \pm (0,2q,0)$ and $\boldsymbol{\tau}_{\mathrm{even}} \pm (0,4q,0)$, respectively. In the case of $\delta_{\mathrm{mag}} \neq 0, \pi$, satellite peaks corresponding to the $2q$ modulation appear, in addition to the above peaks, at $\boldsymbol{\tau}_{\mathrm{odd}} \pm (0,2q,0)$. By substituting $\delta_{\mathrm{mag}} = 76°$, the ratio of the intensities of the spectra, $|P(\boldsymbol{\tau}_{\mathrm{even}} \pm (0,2q,0))|^2$ and $|P(\boldsymbol{\tau}_{\mathrm{odd}} \pm (0,2q,0))|^2$, is calculated to be

$$\frac{|P(\boldsymbol{\tau}_{\mathrm{even}} \pm (0,2q,0))|^2}{|P(\boldsymbol{\tau}_{\mathrm{odd}} \pm (0,2q,0))|^2} = 0.062. \tag{7}$$

This suggests that in x-ray measurements, the satellite reflections corresponding to the $2q$ modulation should be mainly observed at the reciprocal lattice position of $\boldsymbol{\tau}_{\mathrm{odd}} \pm (0,2q,0)$. This shows good agreement with the results of the present

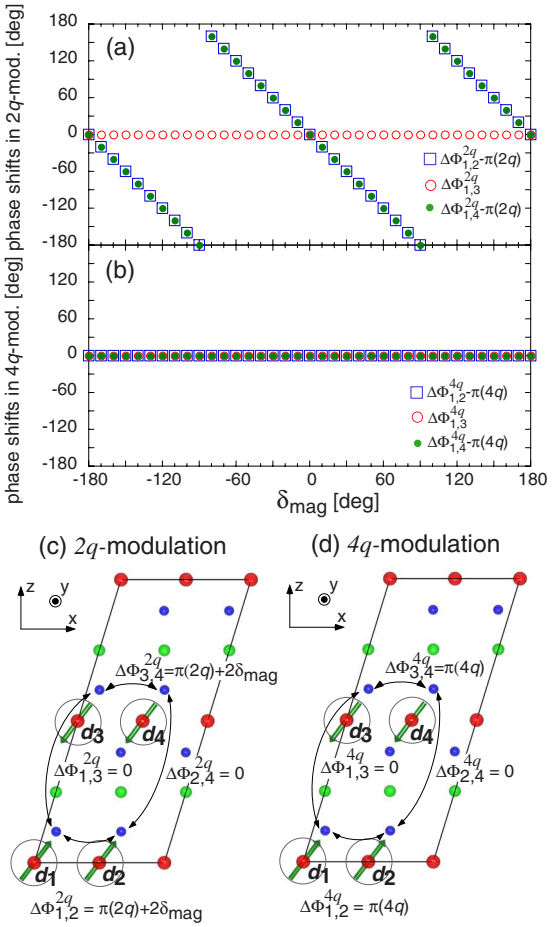

FIG. 7. (Color online) [(a)–(b)] δ_{mag} dependence of the difference between the phases of (a) $2q$ and (b) $4q$ modulations. [(c)–(d)] The phase differences of the (c) $2q$ and (d) $4q$ components in the spatial modulations in the local electric polarization.

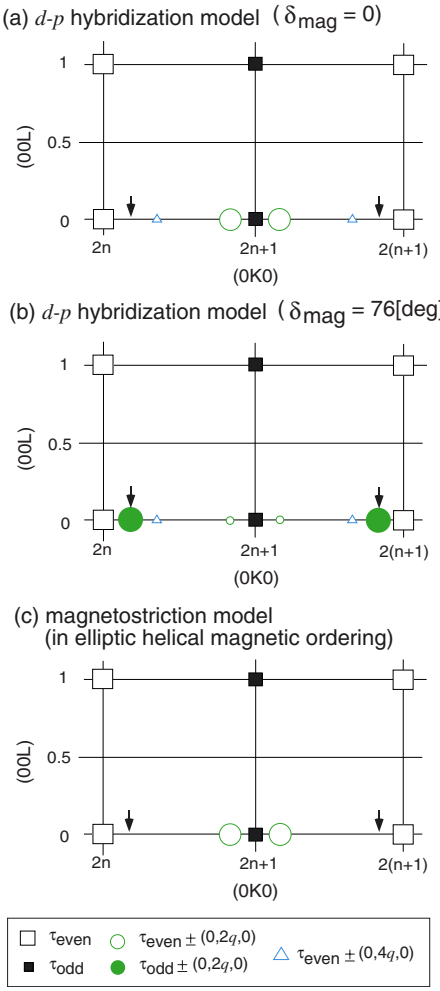

FIG. 8. (Color online) Fourier spectrum mappings of the spatial modulations in the local polarization, which are calculated using (a) the *d-p* hybridization model with $\delta_{\mathrm{mag}}=0,\pi$, (b) that with $\delta_{\mathrm{mag}}=76°$, and (c) the magnetostriction model with finite ellipticity. The size of a symbol, except for $\boldsymbol{\tau}_{\mathrm{even}}$ and $\boldsymbol{\tau}_{\mathrm{odd}}$, qualitatively shows the intensity of the spectrum $|P(\boldsymbol{Q})|^2$, which is normalized by the intensity of the strongest peak in the spectrum. The black arrows denote the position of the satellite reflections observed in the zero-field FEIC phase.

measurements. Although reflections at $\boldsymbol{\tau}_{\mathrm{even}}\pm(0,2q,0)$ and $\boldsymbol{\tau}_{\mathrm{even}}\pm(0,4q,0)$ were not observed in the present measurements, this can be ascribed to the S/N of the present measurements, because the intensities of those reflections are estimated to be much smaller than that of $\boldsymbol{\tau}_{\mathrm{odd}}\pm(0,2q,0)$ reflections.

It should be noted that this result does not change in the parameter region of $0<\alpha<1$, although we assumed $\alpha=0.1$ in the above calculation. This is because the value of α affects only the ratio between the amplitude of the $2q$ modulation and that of the $4q$ modulation (and uniform polarization); specifically, $|P(\boldsymbol{\tau}_{\mathrm{even}}\pm(0,4q,0))|^2/|P(\boldsymbol{\tau}_{\mathrm{odd}}\pm(0,2q,0))|^2$ is in the order of $\sim\alpha^2C'^2(\ll 1)$.

It is worth mentioning here that neither the magnetostriction model nor the spin-current model explains the satellite reflections at $\boldsymbol{\tau}_{\mathrm{odd}}\pm(0,2q,0)$, even if the magnetic structure has finite ellipticity. The spin-current term, $\boldsymbol{e}_{i,i+1}\times(\boldsymbol{S}_i\times\boldsymbol{S}_{i+1})$, does not produce the helical-axis component of the local polarization vector in the proper (or elliptic) helical magnetic ordering in this system. Therefore, the lattice modulations induced by this term do not contribute to the satellite reflection in the reciprocal lattice position of $(0,K,0)$. The magnetostriction term, $(\boldsymbol{S}_i\cdot\boldsymbol{S}_{i+1})$, produces the spatial modulation with a wave number of $2q$ in the helical-axis components of the local polarization vectors when the magnetic structure has finite ellipticity.[21] However, as discussed by Terada *et al.*,[21] the satellite reflections corresponding to the magnetostriction-induced $2q$ modulation are observed only at the reciprocal lattice position of $\boldsymbol{\tau}_{\mathrm{even}}\pm(0,2q,0)$ regardless of the value of δ_{mag} [see Fig. 8(c)]. Therefore, we conclude that the origin of the $2q$-lattice modulation observed in the zero-field FEIC phase is the variation in the metal-ligand hybridization with spin-orbit coupling, which corresponds to feature (iii) mentioned in the Sec. I.

We should mention the nonmonotonic temperature variation of the intensity of the $\boldsymbol{\tau}_{\mathrm{odd}}\pm(0,2q,0)$ reflection observed in the present measurement [see Fig. 4(f)]. The *d-p* hybridization between the Fe^{3+} ions and the O^{2-} ions must depend on the length of the Fe-O bonds, as well as the angle between the Fe-O bond direction and the magnetic moment at the Fe site. We therefore anticipate that the temperature variations of the lattice constants and the fractional coordinates of the oxygen sites affect the temperature variation of the intensity of the $\boldsymbol{\tau}_{\mathrm{odd}}\pm(0,2q,0)$ reflection. The precise determination of the structural parameters by high-resolution x-ray and/or neutron diffraction measurements is desirable for further clarification.

C. Calculation results for an applied field

When a magnetic field is applied along the *b* axis, the magnetic structure is expected to be a conical structure. We also numerically calculated the Fourier spectra for the nonuniform polarizations induced by the conical magnetic structure. Figures 9(a) and 9(b) show the calculation results with the parameters of $\alpha=0.1$ and $\delta_{\mathrm{mag}}=76°$. θ is the angle defined in Fig. 5(a). With increasing θ, the intensities of the Fourier spectra for $2q$ and $4q$ modulations decrease. In the region of $0<\theta<\frac{\pi}{2}$, $1q$ and $3q$ modulations emerge from the first and second terms of Eq. (3), respectively. In reciprocal lattice space, the satellite peaks corresponding to the $1q$ modulations appear at $\boldsymbol{\tau}_{\mathrm{even}}\pm(0,q,\frac{1}{2})$ and $\boldsymbol{\tau}_{\mathrm{odd}}\pm(0,q,\frac{1}{2})$, and the satellite peaks corresponding to the $3q$ modulations appear at $\boldsymbol{\tau}_{\mathrm{even}}\pm(0,3q,\frac{1}{2})$ and $\boldsymbol{\tau}_{\mathrm{odd}}\pm(0,3q,\frac{1}{2})$, as shown in Fig. 9(b).

According to the results of recent magnetization measurements,[31] the canting angle θ at $H_{\|b}=4$ T is roughly estimated to be $5°\sim10°$. In the region of $\theta<10°$, $|P(\boldsymbol{\tau}_{\mathrm{odd}}\pm(0,2q,0))|^2$ decreases slightly with increasing θ, and the intensities of the other Fourier spectra are quite small compared to $|P(\boldsymbol{\tau}_{\mathrm{odd}}\pm(0,2q,0))|^2$, as shown in Fig. 9(a). Hence, it is expected that the intensity of the $\boldsymbol{\tau}_{\mathrm{odd}}\pm(0,2q,0)$ satellite reflection decreases slightly with increasing applied magnetic field along the *b* axis. This is consistent with the results of the present measurements. Although we could not

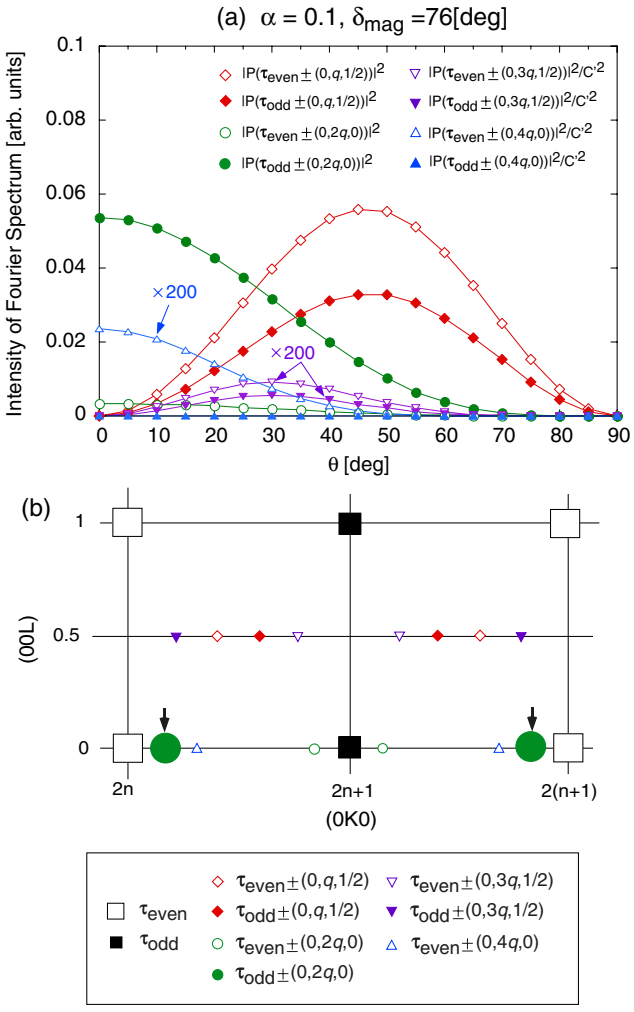

FIG. 9. (Color online) (a) θ dependence of the intensities of the Fourier spectra for the spatial modulations in the local polarization. To enhance the visibility, the data of $3q$ and $4q$ are magnified by a factor of 200. (b) Fourier spectrum mapping of the spatial modulations in the local polarization, which are calculated with the d-p hybridization model with $\delta_{\mathrm{mag}}=76°$, $\alpha=0.1$, and $\theta=10°$. The size of the symbols, except for $\boldsymbol{\tau}_{\mathrm{even}}$ and $\boldsymbol{\tau}_{\mathrm{odd}}$, corresponds to the intensity of the spectrum $|P(\boldsymbol{Q})|^2$, which are normalized using the intensity of the most intense peak in the spectrum. The black arrows denote the positions of the satellite reflections observed in the present measurements.

survey the region of $\theta>10°$, where remarkable changes in the amplitudes of the lattice modulations are expected, these results imply that the d-p hybridization model still works for a finite magnetic field along the b axis.

V. SUMMARY

In summary, we have performed synchrotron radiation x-ray and neutron diffraction measurements under zero field and applied field on the delafossite multiferroic $CuFe_{1-x}Al_xO_2$ with $x=0.0155$, in which the ferroelectric phase shows up under zero field. We found that the threefold rotational symmetry along c_h axis vanishes in the PD and FEIC phases. Although the present result does not determine the symmetry of the crystal structure in the PD and FEIC phases, it is reasonable to propose that a monoclinic lattice distortion occurs in the FEIC and PD phases in $CuFe_{1-x}Al_xO_2$ with $x=0.0155$ because the monoclinic lattice distortion is observed in the PD and FEIC phases in undiluted $CuFeO_2$.[22,24,25] On the other hand, monoclinic lattice distortion was not observed in the OPD phase, which never shows up without nonmagnetic substitution. This implies that the OPD magnetic ordering is stabilized not by the coherent bond order due to magnetostriction, but by the local symmetry breaking due to site-random magnetic vacancies.

In the FEIC phase, we found satellite reflections identified as $\boldsymbol{\tau}_{\mathrm{odd}}\pm(0,2q^{\mathrm{FEIC}},0)$ under zero field. This indicates that the FEIC phase is essentially accompanied by $2q$-lattice modulations. We have calculated the Fourier spectra of the spatial modulations in the local electric polarization using the experimentally determined magnetic structure in the FEIC phase and the microscopic model presented by Arima.[18] Comparing the experimental results with the calculated Fourier spectrum, we revealed that the origin of the $2q$-lattice modulation is not conventional magnetostriction, but the variation in the d-p hybridization between the magnetic Fe^{3+} ions and the ligand O^{2-} ions. Combining the present results with the results of a previous polarized neutron diffraction study,[12] we conclude that the microscopic origin of the ferroelectricity in this system is the variation in the d-p hybridization with spin-orbit coupling.

ACKNOWLEDGMENTS

The authors are grateful to T. Arima and S. Onoda for helpful discussions about the mechanism of the microscopic spin-polarization coupling, and are also grateful to N. Nagaosa for suggesting the importance of the lattice modulations in a new class of magnetoelectric multiferroics. The neutron diffraction measurement at BENSC was carried out along the proposal PHY-01-2285-DT. The synchrotron radiation x-ray diffraction measurements at SPring-8 were performed along the proposal 2007B3773 (BL22XU) with the approval of the nanotechnology network project, and the proposal 2006B1348 (BL46XU). This work was supported by a Grant-in-Aid for Scientific Research (C), No. 19540377, from JSPS, Japan. The images of the crystal and magnetic structures in this paper were depicted using the software VESTA[32] developed by K. Momma.

*nakajima@nsmsmac4.ph.kagu.tus.ac.jp

[1] T. Kimura, T. Goto, H. Shintani, K. Ishizaka, T. Arima, and Y. Tokura, Nature (London) **426**, 55 (2003).
[2] H. Katsura, N. Nagaosa, and A. V. Balatsky, Phys. Rev. Lett. **95**, 057205 (2005).
[3] M. Kenzelmann, A. B. Harris, S. Jonas, C. Broholm, J. Schefer, S. B. Kim, C. L. Zhang, S.-W. Cheong, O. P. Vajk, and J. W. Lynn, Phys. Rev. Lett. **95**, 087206 (2005).
[4] T. Arima, A. Tokunaga, T. Goto, H. Kimura, Y. Noda, and Y. Tokura, Phys. Rev. Lett. **96**, 097202 (2006).
[5] G. Lawes, A. B. Harris, T. Kimura, N. Rogado, R. J. Cava, A. Aharony, O. Entin-Wohlman, T. Yildrim, M. Kenzelmann, C. Broholm, and A. P. Ramirez, Phys. Rev. Lett. **95**, 087205 (2005).
[6] K. Taniguchi, N. Abe, T. Takenobu, Y. Iwasa, and T. Arima, Phys. Rev. Lett. **97**, 097203 (2006).
[7] Y. Yamasaki, S. Miyasaka, Y. Kaneko, J.-P. He, T. Arima, and Y. Tokura, Phys. Rev. Lett. **96**, 207204 (2006).
[8] B. Lorenz, Y.-Q. Wang, and C.-W. Chu, Phys. Rev. B **76**, 104405 (2007).
[9] M. Kenzelmann, G. Lawes, A. B. Harris, G. Gasparovic, C. Broholm, A. P. Ramirez, G. A. Jorge, M. Jaime, S. Park, Q. Huang, A. Ya. Shapiro, and L. A. Demianets, Phys. Rev. Lett. **98**, 267205 (2007).
[10] T. Kimura, J. C. Lashley, and A. P. Ramirez, Phys. Rev. B **73**, 220401(R) (2006).
[11] T. Nakajima, S. Mitsuda, S. Kanetsuki, K. Prokes, A. Podlesnyak, H. Kimura, and Y. Noda, J. Phys. Soc. Jpn. **76**, 043709 (2007).
[12] T. Nakajima, S. Mitsuda, S. Kanetsuki, K. Tanaka, K. Fujii, N. Terada, M. Soda, M. Matsuura, and K. Hirota, Phys. Rev. B **77**, 052401 (2008).
[13] S. Mitsuda, H. Yoshizawa, N. Yaguchi, and M. Mekata, J. Phys. Soc. Jpn. **60**, 1885 (1991).
[14] S. Mitsuda, M. Mase, K. Prokes, H. Kitazawa, and H. A. Katori, J. Phys. Soc. Jpn. **69**, 3513 (2000).
[15] O. A. Petrenko, G. Balakrishnan, M. R. Lees, D. M. Paul, and A. Hoser, Phys. Rev. B **62**, 8983 (2000).
[16] S. Kanetsuki, S. Mitsuda, T. Nakajima, D. Anazawa, H. A. Katori, and K. Prokes, J. Phys.: Condens. Matter **19**, 145244 (2007).
[17] S. Seki, Y. Yamasaki, Y. Shiomi, S. Iguchi, Y. Onose, and Y. Tokura, Phys. Rev. B **75**, 100403(R) (2007).
[18] T. Arima, J. Phys. Soc. Jpn. **76**, 073702 (2007).
[19] C. Jia, S. Onoda, N. Nagaosa, and J. H. Han, Phys. Rev. B **74**, 224444 (2006).
[20] C. Jia, S. Onoda, N. Nagaosa, and J. H. Han, Phys. Rev. B **76**, 144424 (2007).
[21] N. Terada, S. Mitsuda, Y. Tanaka, Y. Tabata, K. Katsumata, and A. Kikkawa, J. Phys. Soc. Jpn. **77**, 054701 (2008).
[22] F. Ye, Y. Ren, Q. Huang, J. A. Fernandez-Baca, Pengcheng Dai, J. W. Lynn, and T. Kimura, Phys. Rev. B **73**, 220404(R) (2006).
[23] T. R. Zhao, M. Hasegawa, and H. Takei, J. Cryst. Growth **166**, 408 (1996).
[24] N. Terada, S. Mitsuda, H. Ohsumi, and K. Tajima, J. Phys. Soc. Jpn. **75**, 023602 (2006).
[25] N. Terada, Y. Tanaka, Y. Tabata, K. Katsumata, A. Kikkawa, and S. Mitsuda, J. Phys. Soc. Jpn. **75**, 113702 (2006).
[26] N. Terada, S. Mitsuda, T. Fujii, K. Soejima, I. Doi, H. A. Katori, and Y. Noda, J. Phys. Soc. Jpn. **74**, 2604 (2005).
[27] N. Terada, T. Kawasaki, S. Mitsuda, H. Kimura, and Y. Noda, J. Phys. Soc. Jpn. **74**, 1561 (2005).
[28] T. Nakajima, S. Mitsuda, S. Kanetsuki, M. Yamano, S. Iwamoto, H. Mitamura, H. A. Katori, K. Prokes, and A. Podlesnyak (unpublished).
[29] In both of the x-ray and neutron diffraction measurements, $H_{\|b}$-increasing scans were performed after zero-field cooling, in which the high-temperature PD phase coexists with the FEIC phase. However, we should mention that the same $H_{\|b}$ dependence of the FEIC magnetic Bragg reflection is observed in the single FEIC phase, which is prepared by the cooling process with an applied field along $[001]_h$ axis.
[30] The many-body effect can be introduced as $C_0(1+C'\cos 2\Theta_{1,1})(1-\alpha C'\cos 2\Theta_{2,1})(1-\alpha C'\cos 2\Theta_{4,1})$. Here, we neglect the term $O(\alpha^2)$, and obtain Eq. (2).
[31] H. A. Katori, S. Kanetsuki, N. Terada, S. Mitsuda, H. Mitamura, K. Kindo, and S. Takeyama (unpublished).
[32] K. Momma and F. Izumi, J. Appl. Crystallogr. **41**, 653 (2008).